Investigating the Performance of a Novel Multi-Element Airfoil Concept Using Numerical Analysis

Kareem Ahmed Ismail Elsafty[1],*, Atif Mohamed Emad Elsherif[1], Ahmed Abdelhamid Ibrahim[1], Omar Sherif Mohamed[1], Ahmed Mohamed Reda Elbaz[1]

[1] Centre for Renewable Energy-Wind Energy Division, The British University in Egypt, Cairo, Egypt

ARTICLE INFO	ABSTRACT
	Separation control is one of the trending topics recently for Vertical Axis Wind Turbine (VAWT) applications, flow separation that occur on the suction side of an airfoil is a major limitation for VAWTs starting and power coefficient; passive control of flow separation has been attracting wind energy research community recently. The principle objective of this paper is to investigate the effect of the multi-element airfoil on the aerodynamic characteristics at wide range of angles of attack at a Reynolds number of 140,000. The multi element airfoil modification has been implemented by replacing the baseline airfoil with two airfoil members within the same geometrical profile of the original baseline airfoil, cambered and symmetrical airfoil members were investigated in this work. The cambered airfoil sections were made of the NACA 4412 airfoil while the symmetrical airfoil sections consisted of the NACA 0015 airfoil. The baseline airfoil is a profile of NACA 0021. The numerical investigation was executed using computational fluid dynamics (CFD) by the usage of ANSYS FLUENT and the turbulence model used was the k-ε Standard. The results of the present research show that the optimized multi-element airfoil configurations have better performance than the baseline airfoil at high angles of attack. A significant delay of separation was observed using the multi element airfoil, resulted in an increase of 200% in the glide ratio using cambered airfoil members and of 100% using symmetric airfoil members. These results are expected to have a significant effect on the performance of low wind speed wind turbines. In addition, a potential benefit for vertical axis wind turbines, whereas the airfoil generates lift at wider range of angles of attack.

1. Introduction

Wind turbines are becoming an essential part of today's energy sources. Majority of efficient wind turbines utilize airfoils to generate thrust that rotates the turbine. The theory of airfoil is to generate high lift force with minimum drag force, thus contribute to the thrust. With the Energy growing demand, wind turbine research focuses mostly on the need to construct more efficient and larger wind turbines. However, structural obstacles start to appear when the rotor blades' swept area

---

increases as when the volume of the blades increases the weight increases. Thus, multi element airfoil systems are used to enhance the aerodynamic performance and overcome the problem of conflict structural requirements and aerodynamic requirements [1,2]. Many studies on the potential benefits of the multi element airfoil systems have been performed [3-5]. Thick airfoils such as the DU 00-W-401 airfoil geometry which is a wind turbine airfoil with a thickness of 40.1 % constructed in 2000 by the University of Delft was used as reference geometry for the multi element configurations in many studies [4,6]. Different combinations of struts, flaps and slats were set up around the main airfoil element in these configurations where each element is represented by a letter. ANSYS FLUENT was used to perform a CFD analysis by Narsipur *et al.,* [6] on the geometry of MFF-089 multi element shown in Figure 1 at a Reynolds number of 1,000,000. During examination of various overhangs, deflection angles and gaps the lift coefficient CL increased when the deflection of flapped increased. For drag coefficient there were small changes with flap deflection variabilities. Drag and lift were affected significantly by the variations in overhang flap gap. Negative effect had been reported when the distances of overhang and gap sizes were reduced because of the wake bursting increase. The probability of flow reversal is increased by the flow acceleration through the gaps of the flap.
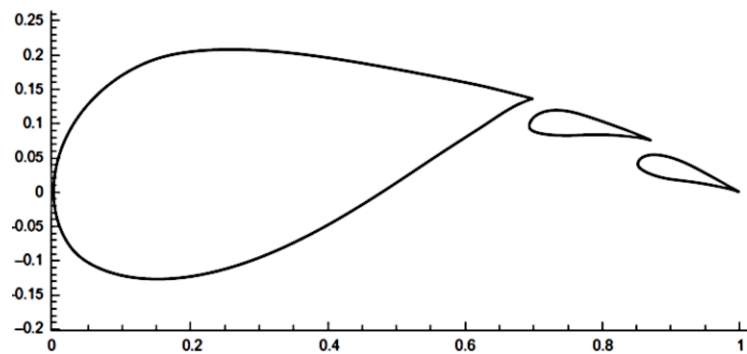
Fig. 1. Multi element airfoil geometry of MFF-089 [6]

Another configuration involves a thin main element with two flaps and a strut under the main element component. the lower spar cap is represented by the strut element and the upper spar cap is represented by the main element. The convection MFFS was given to this configuration the (M) refers to the main element, the (FF) refers to the two flaps and the (s) refers to the strut. The MFFS-018 arrangement which is represented in Figure 2 from Ragheb and Selig's [4] study evolved the MFFS family.
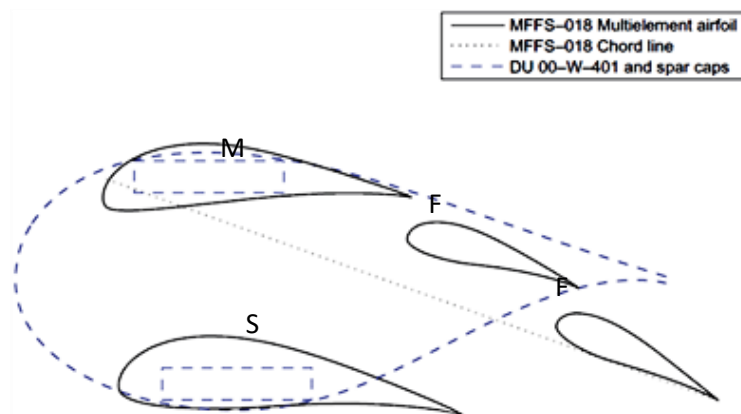
Fig. 2. Airfoil geometry of MFFS-018 multi element airfoil [4]

Compared to the airfoils' family of Delft university, The MFFS-018 provide an increased CL/CD with values of CL reaching 1.7 [7]. The MFFS-018 had been established to increase the lift even further over the lift of a single flap configuration. At Reynolds number of 3,000,000 the DU 00-W-401 airfoil had a maximum lift to drag ratio (CL/CD) of 83 at a lift coefficient of 1.04 and an angle of attack of 6.5 which is slightly less than the lift to drag ratio provided by the MFFS-018 with a maximum CL/CD of 158 at lift coefficient of 2.34. Among the various configurations which have been analysed by Ragheb and Selig [4], the MFFS-018 appears to have the highest maximum CL/CD as shown in Table 1.

Table 1
Summary of different multielement configuration [4]

Airfoil	$C_l/C_{d_{max}}$	C_l at $C_l/C_{d_{max}}$	% increase in $C_l/C_{d_{max}}$
DU 00-W-401	82.9	1.04	-
MFS-004	152.9	2.42	84.4
MFS-104	156.1	2.42	88.3
MFFS-018	158.0	2.34	90.5
SMFS-004	150.4	2.82	81.4
MSS-001	116.9	1.77	41.0
MSS-102	121.1	2.01	46.1
MFSF-006	128.4	2.99	54.9

Atalay *et al.,* [8] investigated the performance of the multielement airfoil system at which NACA 4412 is the main element and NACA 6411 represents a slat at leading edge as shown in Figure 3.
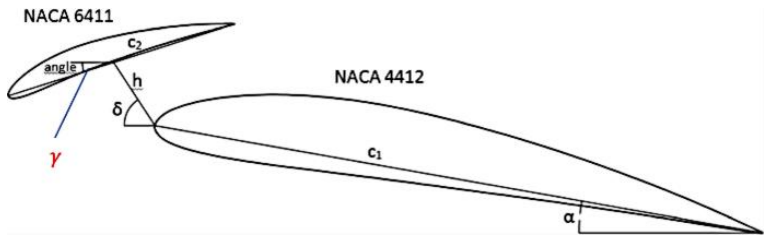
Fig. 3. NACA 6411 and NACA 4412 leading-edge slat design [8]

It has been found that the optimum parameter for the maximum CL/CD value are γ = 52.5o, α = 10.5o, δ = 23.5o, h/c2 = 0.26, and c2/c1 = 0.34. The value of the maximum CL/CD ratio obtained is 25.1.

The possible advantages of adding slats to the wind turbine have been discussed by many studies [9-11]. A computational investigation has been conducted by Gaunaa *et al.,* [12] to rotor slats for the system described by 0.1 ⬚ r/R ⬚ 0.3 For a reference of 10 MW wind turbine base line light rotor. Where, (R) is the rotor radius, (r) is the radial location on the rotor. It has been detected using 3D CFD that there is a major change in the inner region of the rotor's flow field. The CP has increased by 1% with a CT corresponding increase by 2%. Another study performed by Jaume *et al.,* [13] investigated the performance of DU91-W2-250 airfoil with mounted slat upon it. The airfoil is 25% thick and is located at r/R = 43%. The results of the investigation showed an increase of the angle of attack range at which the airfoil behaved well. Furthermore, there was a 9 degree increase of the critical angle of attack and 64.8% increase of the maximum lift coefficient.

In this paper numerous attempts were conducted to maximize the lift generation as well as minimizing the drag on the airfoil, especially at low Reynolds number where the applications of vertical axis wind turbines are common. In more details, the current work aims at creating a multi-element of airfoils to replace the single airfoil, optimizing this technique would delay the flow

separation and enhance the airfoil performance. The new concept is applied to NACA 0021 by splitting the airfoil section into a cascade of two airfoils of smaller chord length. Several attempts have been carried out to reach a better glide ratio at low Reynolds number.

The work shown in this paper had been conducted by the usage of ANSYS Fluent as it had recently demonstrated its competency in gaining reliable results when it comes to lift and drag coefficients in comparison to experimental wind tunnel results especially at relatively low Reynolds number as per Khan *et al.,* [14], which contributes directly in saving massive cost and time.

2. Numerical Methodology

The domain created for the baseline airfoil and multi element airfoil modification configurations is presented in Figure 7. As can be shown, a C-domain type had been chosen for all upcoming simulations as it provides a major ability of varying the angle of attack by the alteration of the incoming air flow direction by the usage of the semi-circular inlet boundary with no need to vary the orientation of the airfoil. The dimensions of the domains tested can be shown in Table 2, as well as, the results of coefficient of lift and glide ratio to each of the investigated domains. The domain dimensions were introduced in terms of the chord length (C) of the baseline airfoil. As it can be observed in Table 2, the dimensions of the domain had a slight effect on the results of the coefficient of lift while the glide ratio was more responsive to the changes in the domain dimensions. It was clear that the domain dimensions affect the results obtained from the simulation as small domains restrict the development of the air flow and huge domains will have an unnecessary number of nodes. Therefore, a domain that does not affect the results will be chosen and, in this case, increasing the domain dimensions beyond domain number 4 has an unnoticeable effect on the glide ratio results. Therefore, the chosen domain is domain number 4 ensuring that the results are free of domain error. The Reynolds number used for mesh test is 360,000 and the velocity can be obtained via the following equation.

Reynolds Number Equation [15]

$$Re = \frac{\rho V c}{\mu} \tag{1}$$

Table 2
Domain Test Results

Domain Number	Upwind	Downwind	Cl	Cl/Cd
1	5C	10C	0.7973	29.25
2	10C	20C	0.7971	30.48
3	15C	30C	0.7982	31.01
4	20C	40C	0.79792	31.22
5	25C	50C	0.79616	31.20

The created domain had to be discretised into small subdomains in which computations take place. A grid independency test had to be executed in order to choose the finest mesh data that provide results free form mesh errors. The mesh details can be witnessed in Figure 8 and the mesh test results can be witnessed in Table 3. The number of nodes and the number of layers had been altered in the quest for the optimum mesh data and the corresponding coefficient of lift and glide ratio results had been recorded. As it can be noticed form Table 3, mesh number 1 is the one that affects the coefficient of lift result the most while other mesh data affect the coefficient of lift results slightly while the glide ratio had been affected considerably until mesh number 3. Therefore, mesh

number 3 carry the mesh data chosen for the upcoming simulations conducted in this paper. The mesh data chosen had a maximum skewness value of 0.58997 and an aspect ratio of 13.839. The grid chosen contained an average y+ value of 0.67443 which allows the application of enhanced wall treatment while using k-ε turbulence models and the usage of k-ω SST turbulence model. The mesh test was conducted at a Reynolds number of 360,000.

Table 3
Mesh Test Results

Mesh Number	Number of Nodes	Number of Layers	Cl	Cl/Cd
1	208302	5	0.81485	33.78
2	318795	10	0.79792	31.22
3	356721	20	0.79003	30.17
4	416563	30	0.78993	30.11
5	456031	40	0.79253	30.27

Turbulence model validation was carried out by computing coefficient of lift results by the usage of different turbulence models against experimental data for the baseline NACA 0021 that were extracted from the work of Balduzzi *et al.,* [16] within a range of $0^o \leq AoA \leq 20^o$. A turbulence model validation was conducted to choose a suitable turbulence model that can be used in all upcoming simulations. The turbulence model validation results can be shown in Figure 4. The k-ε Standard was chosen for all further simulations presented in this paper considering its matching with the experimental results. The turbulence model validation was conducted at a Reynolds number of 140,000 as well as the rest of the simulations present in this paper. The convergence criteria of all of the conducted simulations were considered at a low residual level of $10{-}5$ for momentum and turbulence variables. Moreover, a pressure-based solver was used to solve the steady RANS equations considering the low Mach number of the flow, also the pressure and velocity were solved using the Coupled solver to guarantee faster convergence [17]. Second order upwind discretisation scheme was used for minimum numerical diffusion [17].
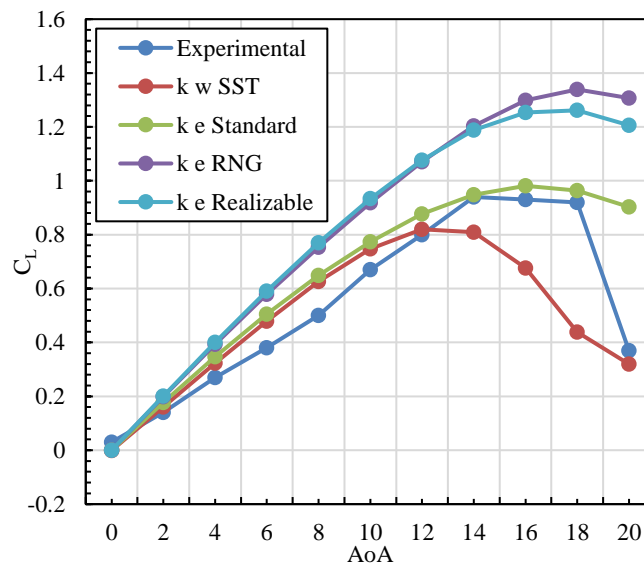
Fig. 4. Turbulence Model Validation Results [16]

3. Multi-Element Airfoil Concept of Operation

The design of multi-element airfoil allows a jet flow to pass from the pressure side to suction side. Thus, accelerating the flow on the suction side of airfoils. This leads to delay the separation at high angles of attack, and hence increased lift force due to the sustained pressure difference between the pressure side and suction side of the airfoil. The concept of multi-element airfoil is similar to the slotted airfoil concept discussed in the study by Mohamed *et al.,* [18]. Multi element airfoils usually include a leading-edge slat or trailing edge flap. By manipulating these two elements, the characteristics of the airfoil can be controlled. The basic idea behind the current study is to modify this concept by splitting a base airfoil into two smaller airfoils at different overlap and inclination angle, within the base airfoil, as shown in Figure 5. In the present work, the NACA 0021 airfoil was selected as the baseline airfoil. The current investigation was performed using Computational Fluid Dynamics (CFD). This technique has been widely used in the recent years with high degree of reliability to predict the aerodynamic behavior around airfoils. The simulations were validated against experimental results of the baseline airfoil at Reynolds number of 140,000 and the turbulence model used is the k-ε Standard. The model was then applied to investigate the new concept of multi element airfoils.
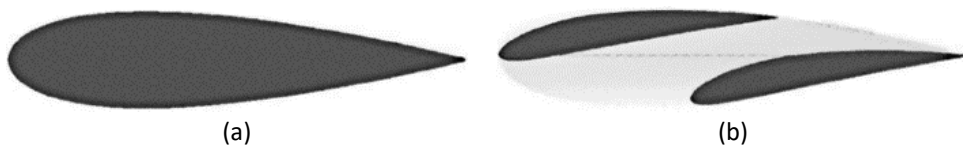
(a)   (b)
Fig. 5. Representation for the airfoil sections: (a) baseline airfoil; (b) proposed multi-element airfoil

3.1 Concept of the Modification

The main idea of this paper is to investigate the effect of applying the multi element airfoil modification using cambered and symmetrical airfoils as the two sections of the modification. The cambered multi element airfoil modification configurations were executed by using the NACA 4412 airfoil as the two members of the modification, while the symmetrical multi element airfoil modification configurations were executed by using the NACA 0015 airfoil as the two members of the modification. There were four factors within the two sections of the modification shown in Figure 6 that were manipulated in many formations in order to reach the optimal configurations and they were c_1, c_2, α_1 and α_2 and these various manipulations were implemented taking into consideration one major constraint and it is not to surpass the geometrical profile of the baseline NACA 0021 airfoil. Many configurations were tested for the cambered and symmetrical multi-element airfoil aiming for optimizing the aerodynamic performance. It was decided to only show four configurations with significant results for both the cambered and symmetrical configurations, as well as all found optimal cambered and symmetrical configurations. Results of lift and drag coefficients variations with the angle of attack were evaluated and compared with the baseline airfoil results. In addition, some further analysis and discussion were carried out for the best optimized case for the cambered and symmetrical configurations in comparison with the baseline airfoil.

Figure 6 shows the detailed description for each factor manipulated of the multi element airfoil modification configurations that were mentioned in this paper. The first factor of the configuration is c_1 which is the chord length of the first element and it is represented by a percentage of the original airfoil chord length, the second factor is c_2 which is the chord length of the second element and it is represented by a percentage of the original airfoil chord length. The third and the fourth factors were

the angles α_1 and α_2, which are the angle between the chord line of the first element and the chord line of the baseline airfoil, and the angle between the chord line of the second element and the chord line of the baseline airfoil, respectively.

Table 4
Detailed description for each factor of the configurations

Configurations	c_1	c_2	α_1	α_2	Members
BL	--	--	--	--	NACA0021
1C	0.5 m	0.4 m	10.8°	11.4°	NACA4412
2C	0.5 m	0.5 m	10.8°	10.6°	NACA4412
3C	0.5 m	0.6 m	10.8°	9.7°	NACA4412
4C	0.6 m	0.5 m	7.7°	10.6°	NACA4412
5C	0.5 m	0.4 m	10.8°	0°	NACA4412
6C	0.5 m	0.4 m	10.8°	-2°	NACA4412
7C	0.4 m	0.5 m	14.8°	0°	NACA4412
8C	0.5 m	0.5 m	10.8°	0°	NACA4412
9C	0.5 m	0.6 m	10.8°	0°	NACA4412
1S	0.4 m	0.6 m	14.8°	0°	NACA0015
2S	0.5 m	0.5 m	10.8°	0°	NACA0015
3S	0.5 m	0.6 m	10.8°	0°	NACA0015
4S	0.6 m	0.5 m	7.7°	0°	NACA0015
5S	0.5 m	0.5 m	8°	-3°	NACA0015
6S	0.5 m	0.5 m	9°	-3°	NACA0015
7S	0.5 m	0.5 m	10°	-3°	NACA0015
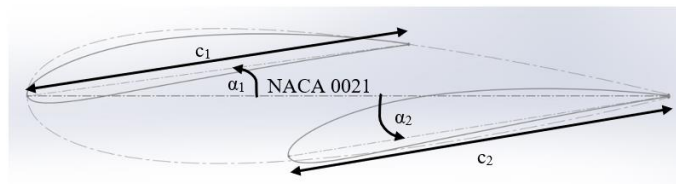
Fig. 6. The factors manipulated in the multi element airfoil modification
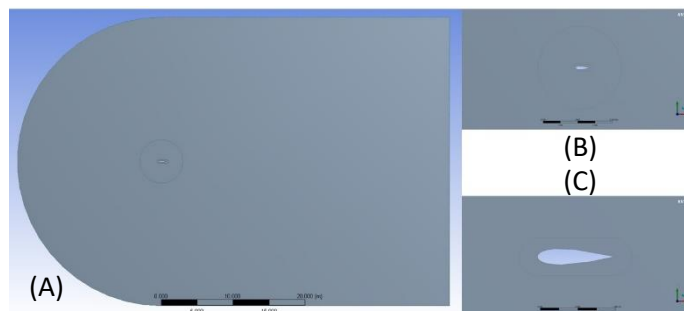
Fig. 7. Airfoil domain details; (A) full domain; (B) circle around the airfoil; (C) oval around the airfoil
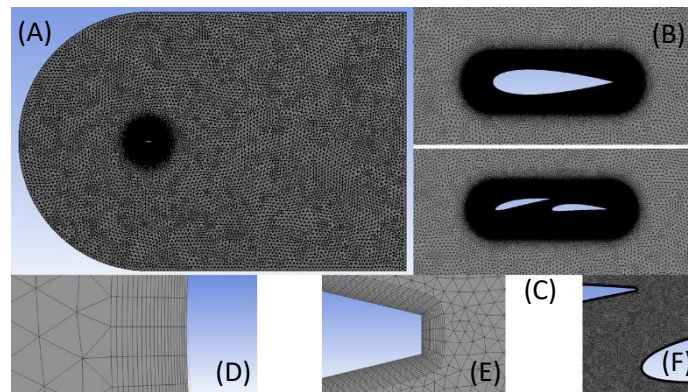
Fig. 8. Airfoil mesh details; (A) full domain; (B) baseline airfoil; (C) multi element airfoil; (D) inflation layers at leading edge; (E) inflation layers at trailing edge; (F) multi element outlet

4. Results and Discussion

The numerical results obtained in this section are the coefficients of lift (CL), the coefficients of drag (CD) and the glide ratios (CL/CD) results of the 16 mentioned multi element airfoil modification configurations. The simulations of the cambered and symmetrical multi element airfoil modification configurations showed promising results. For the cambered airfoil system, the analysis started by maximizing α_1 and α_2 angles while manipulating c_1 and c_2 values creating four essential configurations which are 1C, 2C, 3C and 4C. For the symmetrical multi element airfoil system, the analysis started by maximizing α_1, minimizing α_2 and manipulating the lengths of c_1 and c_2 creating four important configurations which are 1S, 2S, 3S and 4S.

Significant increase in the lift to drag ratio is shown in Figure 9 and Figure 10. The highest glide ratio achieved by cambered members was a value of 26.4 and for the symmetrical members was a value of 23.8 compared to a value of 10.95 for the baseline airfoil. However, it is noticeable that there is a significant decrease of glide ratio at the low angles of attack for both the cambered and symmetrical members of the multi element airfoil. Therefore, the coefficient of lift curves and the coefficient of drag curves for those configurations were analysed to determine the reason behind the presence of negative values of glide ratios at low angles of attack. Figure 11 and Figure 13 indicate that the reason behind the negative glide ratio values at low angles of attack is the presence of negative lift. The presence of negative lift at very low angles of attack is due to the angle inclinations of the two elements that form the configuration and this problem can be solved by manipulating α_1 and α_2 angles to increase the lift at the low angles of attack.
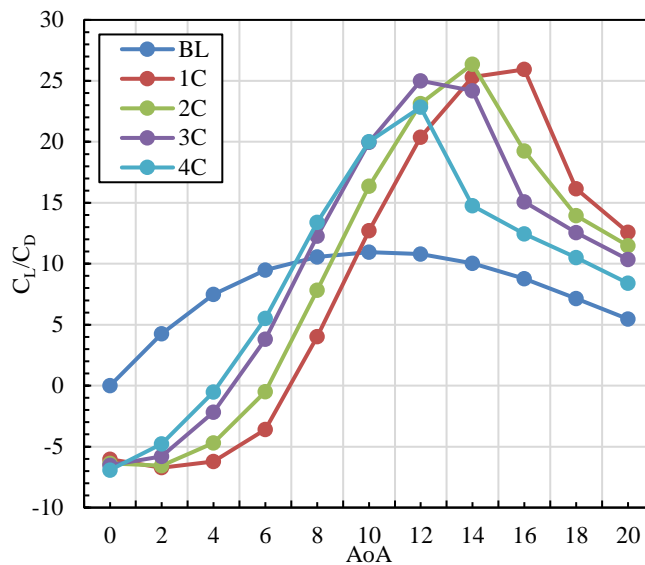
Fig. 9. Glide Ratio curve for the significant cambered multi element airfoil modification configurations
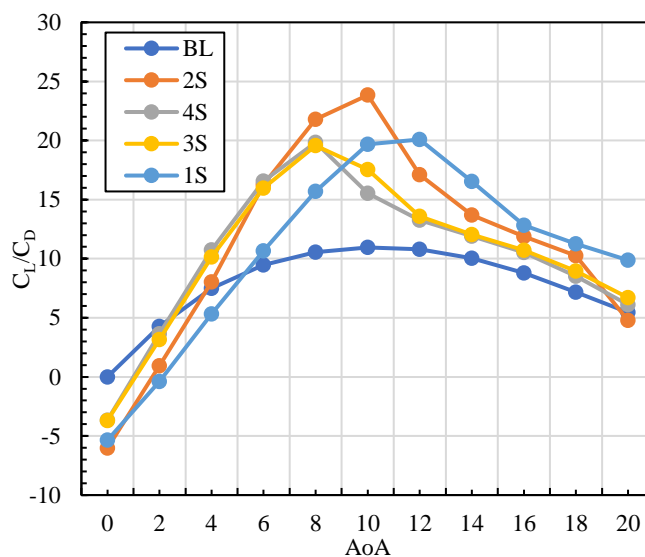
Fig. 10. Glide Ratio curve for the significant symmetrical multi element airfoil modification configurations
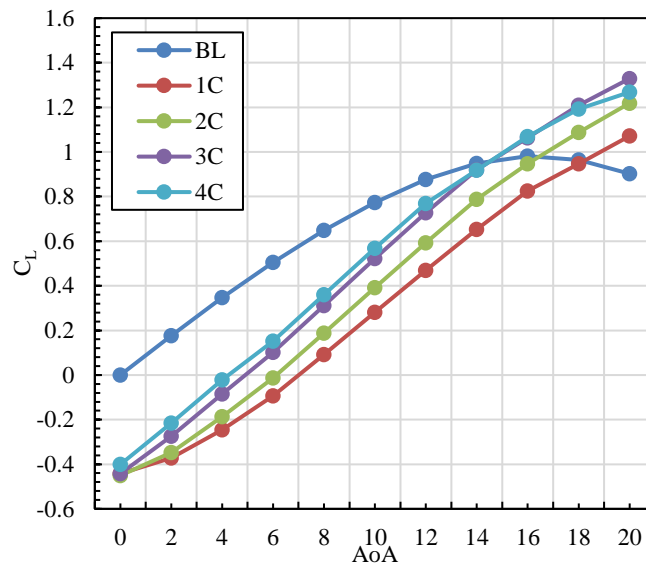
Fig. 11. Coefficient of lift curve for the significant cambered multi element airfoil modification configurations
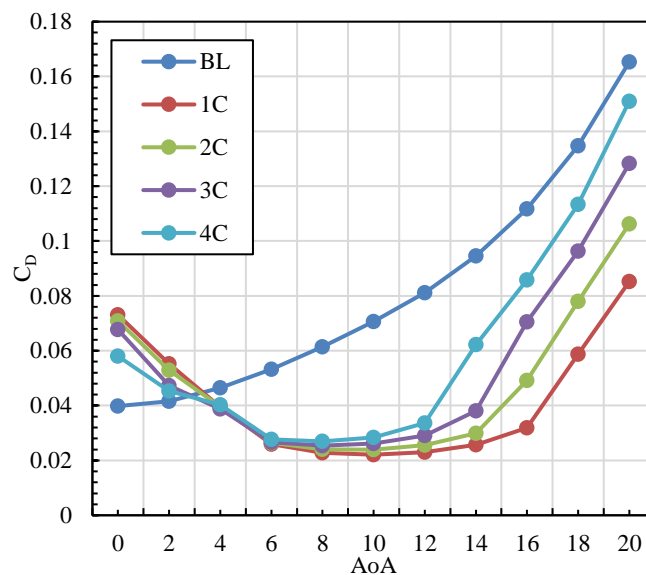
Fig. 12. Coefficient of drag curve for the significant cambered multi element airfoil modification configurations
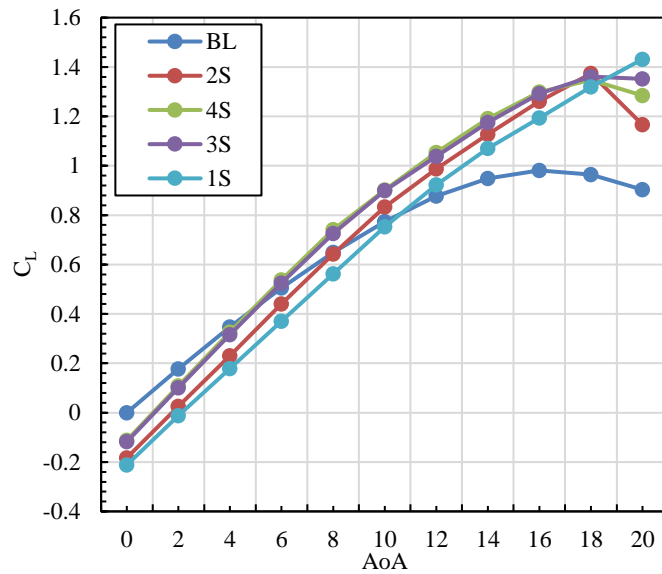
Fig. 13. Coefficient of lift curve for the significant symmetrical multi element airfoil modification configurations
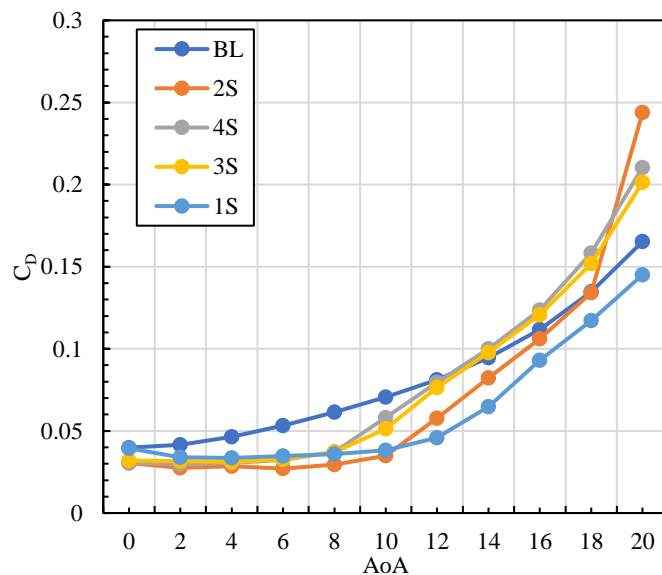
Fig. 14. Coefficient of drag curve for the significant symmetrical multi element airfoil modification configurations

Optimum configurations have been found after manipulating α1 and α2 angles for both cambered and symmetrical multi element airfoil modification configurations. For the cambered multi element airfoil modification configurations, the configurations 5C, 6C, 7C, 8C and 9C have been obtained as the optimal cambered configurations and their glide ratio curves can be shown in Figure 15. It can be noticed in Figure 15 that the optimum cambered configurations were able to raise the whole glide ratio curve in comparison with the baseline NACA 0021 airfoil having a maximum increase of exactly 206.2% for the 8C configuration in comparison with the highest obtainable glide ratio by the baseline NACA 0021 airfoil. For the symmetrical multi element airfoil modification configurations, the configurations 5S, 6S and 7S have been obtained as the optimal symmetrical configurations and their glide ratio curves can be shown in Figure 16. It can be noticed in Figure 16 that the optimum

symmetrical configurations were able to raise the whole glide ratio curve in comparison with the baseline NACA 0021 airfoil having a maximum increase of exactly 137.7% for the 6S configuration in comparison with the highest obtainable glide ratio by the baseline NACA 0021 airfoil. In addition, Figure 15 and Figure 16 clarify that the problem of negative glide ratio values at very low angles of attack had been resolved by finding the optimum positions for angles α1 and α2. The whole glide ratio curves experienced a significant increase in comparison with the baseline airfoil which will have a positive effect on delaying the flow separation angle to a further one. Furthermore, the optimum value of glide ratio had reached a value of 33.53 for the cambered multi element airfoil modification configurations and a value of 26.03 for the symmetrical multi element airfoil modification configurations in comparison to a value of 10.95 for the baseline airfoil at the Reynolds number of 140,000.
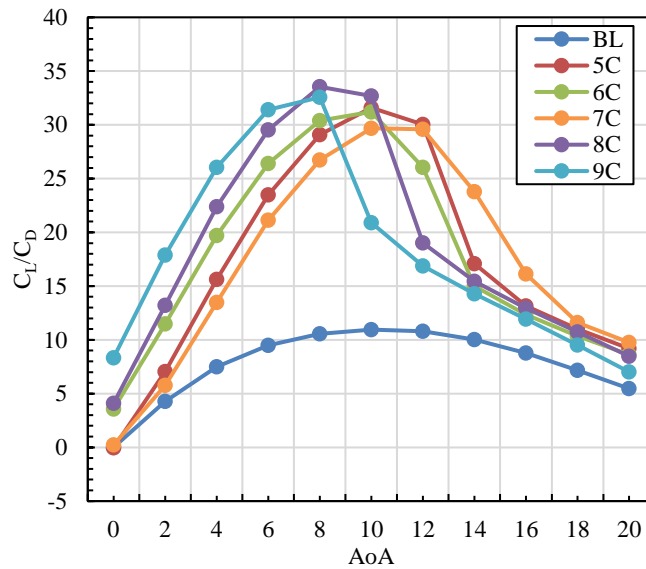
Fig. 15. Glide Ratio curve for the optimal cambered multi element airfoil modification configurations
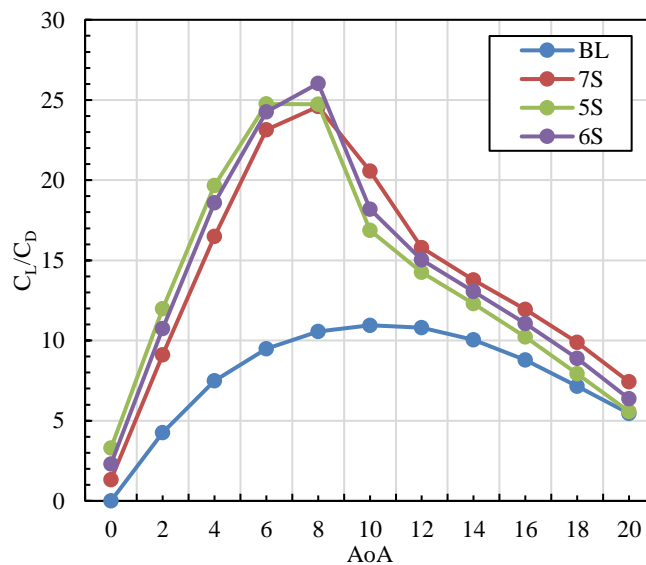
Fig. 16. Glide Ratio curve for the optimal symmetrical multi element airfoil modification configurations

The analysis conducted in this section is related to one cambered multi element airfoil modification configuration and one symmetrical multi element airfoil modification configuration in comparison with the baseline NACA 0021 airfoil and with each other. The cambered one is the 8C configuration and it is the one configuration able to reach the highest value of glide ratio among all other cambered multi element airfoil modification configurations while the symmetrical one is the 6S configuration and it is the one configuration able to reach the highest value of glide ratio among all other symmetrical multi element airfoil modification configurations. The comparison between the three configurations includes coefficient of lift curves, coefficient of drag curves, glide ratio curves, coefficient of pressure curves and velocity contours with streamlines.

Figure 17 shows the coefficients of lift for the 8C and 6S multi element airfoil modification configurations and the baseline NACA 0021 airfoil. It can be noticed the cambered and the symmetrical multi element airfoil modification configurations were able to enhance the coefficient of lift values along the whole range from 0° to 20° angles of attack. The cambered configuration had the highest values of coefficients of lift along the whole range of angles of attack.
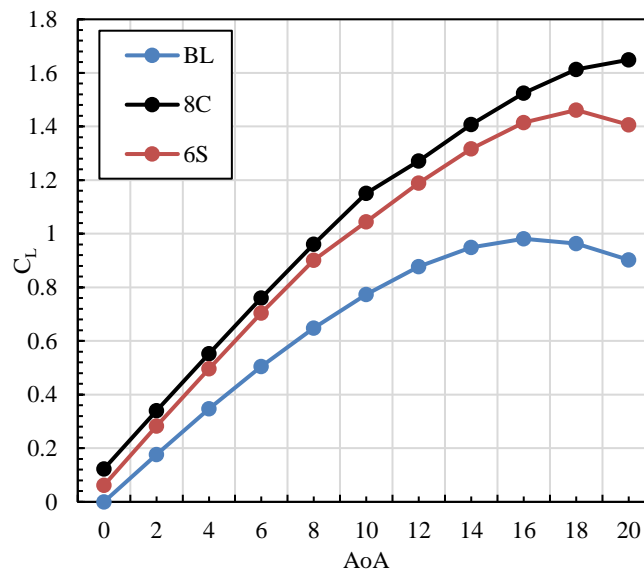
Fig. 17. The coefficients of lift against the angles of attack

Figure 18 reveals the coefficients of drag for the 8C and the 6S multi element airfoil modification configurations and the baseline NACA 0021 airfoil. It can be witnessed that both cambered and symmetrical configurations were able to enhance the coefficients of drag from 0° to 12° angles of attack while having only the cambered configuration enhancing the coefficient of drag at the angle of attack 14°. Both configurations were not able to enhance the coefficient of drag at high angles of attack due to the presence of two bodies of airfoils instead of having a single airfoil body as it is the case with the baseline airfoil.
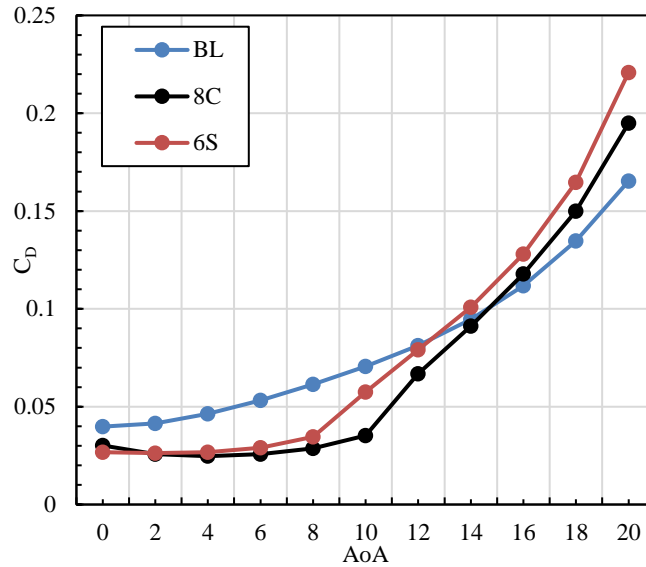
Fig. 18. The coefficients of drag against the angles of attack

Figure 19 shows the glide ratio curves for the 8C and the 6S multi element airfoil modification configurations and the baseline NACA 0021 airfoil. It can be observed that both the cambered and the symmetrical configurations were able to raise the whole glide ratio curve along the whole range of 0° to 20° angles of attack in comparison with the baseline NACA 0021 airfoil. The cambered configuration had better glide ratio values than those of the symmetrical configuration along the whole range of angles of attack. Although those multi element airfoil modification configurations were not able to enhance the coefficients of drag at high angle of attack, the glide ratio is enhanced at high angles of attack. This is due to the fact that the coefficients of lift were highly enhanced at high angles of attack.
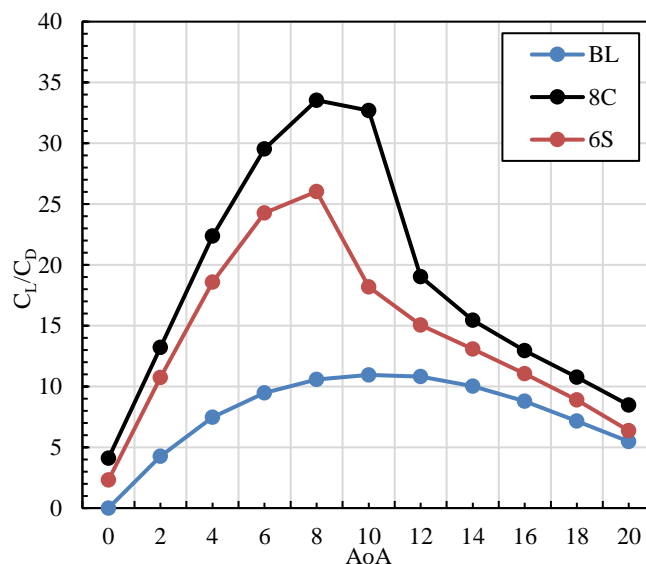
Fig. 19. Glide Ratio curve against angles of attack

Figure 20 shows the coefficient of pressure graph for both sections of the 8C and the 6S multi element airfoil modification configurations as well as the baseline NACA 0021 airfoil section at the angle of attack of 8°. It can be witnessed that both first sections of the cambered and symmetrical

configurations were able to enhance the coefficient of pressure in comparison with the baseline airfoil only at the pressure side of the airfoil while having only the symmetrical configuration enhancing the coefficient of pressure at the pressure side along the whole section. The first section of the cambered configuration was able to maintain a higher pressure difference along its whole section than that offered by the first section of the symmetrical configuration. The second sections of the cambered and symmetrical configurations were able to enhance the overall coefficient of pressure along the whole sections in comparison with the baseline airfoil at both sides of the airfoil, suction side and pressure side. The second section of the symmetrical configuration had a steeper curve than that of the second section of the cambered modification resulting in a better pressure difference for the second section of the cambered modification. This occurred due to the fact that air flows around a second airfoil creating high pressure at the pressure side and high velocity at the suction side for a second time within the same airflow. This behavior justifies the increased lift and decreased drag of the cambered and symmetrical configurations in comparison with the baseline airfoil. The presence of two sections instead of one airfoil created a maintained pressure difference which indicates that the separation loss had been delayed and, in this case, the very gradual decrease in pressure difference approximates the absence of flow separation between the air flow and the suction side of the airfoil for the optimal configurations.
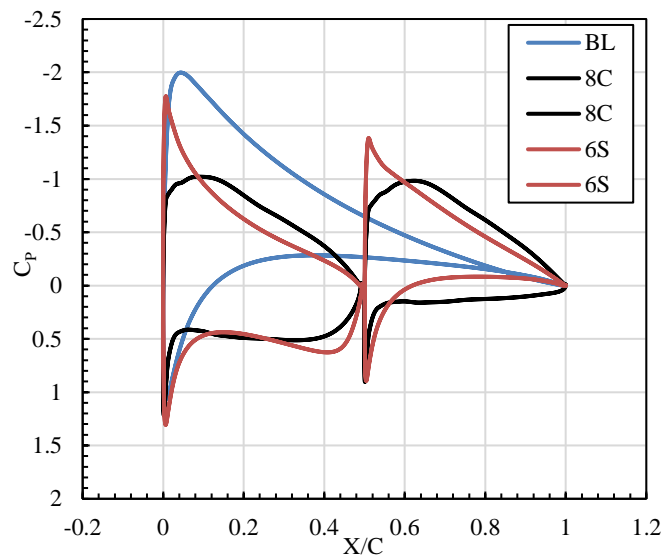
Fig. 20. The coefficient of pressure at angle of attack 8°

Figure 21 shows the coefficient of pressure graph for both sections of the 8C and the 6S multi element airfoil modification configurations as well as the baseline NACA 0021 airfoil at an angle of attack of 16°. The first sections of the cambered and symmetrical configurations were able to enhance the coefficient of pressure along the whole sections in comparison with the baseline airfoil at the pressure side of the airfoil while only the first section of the symmetrical configuration was able to enhance the coefficient of pressure at the suction side but only for a very tine part of the airfoil. The second sections of the cambered and symmetrical configurations were able to also enhance the overall coefficient of pressure along the whole sections in comparison with the baseline airfoil at the suction and pressure sides. The symmetrical configuration was able to reach a lower maximum coefficient of pressure at the suction side in comparison with the cambered configuration and the baseline airfoil while the cambered configuration had a better overall maintenance to the pressure difference in comparison with the symmetrical configuration and the baseline airfoil.
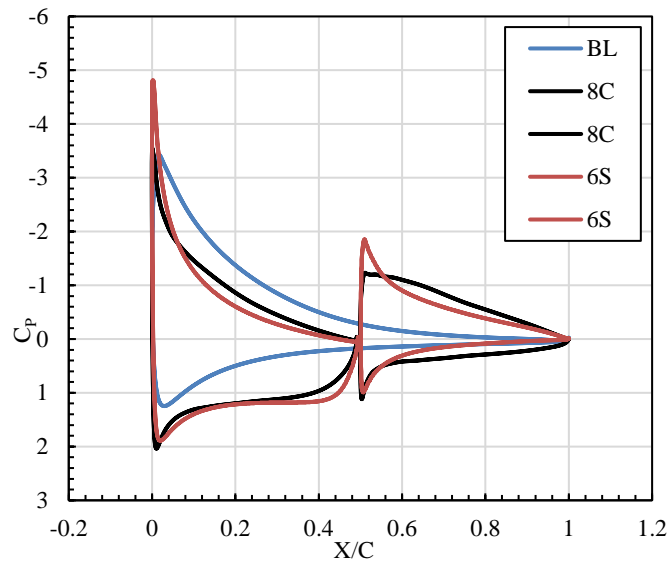
Fig. 21. The coefficient of pressure at angle of attack 16°

The velocity contour in 2D simulations is usually used in order to show the areas that contain the highest values of velocity as well as the areas that contain lowest values of velocity when it comes to the interaction between the air flow and the solid walls that are being analysed and, in this case, the solid walls that are within concern in this analysis are the airfoil surfaces. There are streamlines along the presence of velocity contours and their main aim is to show the direction of air flow around the airfoil and they are extremely essential in noticing the vortices that may occur on the upper surface of an airfoil at its trailing edge due to the separation loss phenomena that take place between the air flowing and the upper surface of the airfoil. The velocity contour and streamlines analysis was conducted at two angles of attack for both cambered and symmetrical configurations as well as for the baseline NACA 0021 airfoil.

As it can be shown in Figure 22, within each and every single airfoil there are three essential areas when it comes to the velocity contours and streamlines, the first area is the area where the velocity is maximum and this area can be found on the upper surface of an airfoil at its leading edge. The second area is an area of very low velocity which can be approximated to zero and it is the area of highest pressure on the airfoil on the lower surface of the airfoil at its leading edge and it is called the stagnation point, while the third area is an area of low velocity and it can be found on the upper surface of an airfoil at its trailing edge and this area is extremely important as it gives an indication about an important factor that affects the aerodynamic performance of an airfoil and it is the separation loss phenomena that occurs between the upper surface of an airfoil and the air flow resulting in the creation of vortices.

Figure 22 shows the effect of applying the multi element airfoil modification by using cambered and symmetrical configurations, respectively. It can be observed in both configurations that the area of low velocity that should appear on the upper surface of the four sections at the trailing edge is nearly eliminated at both angles relative to the baseline airfoil. Therefore, the creation of vortices was not present on any of the modification sections except for the second section of the cambered configuration at AoA 16° that had very slight creation of vortices at the very end of the section on its suction side which indicates that the air flow was extremely attached to the upper surface of the four sections of the two multi element airfoil modification configurations represented in this analysis at both angles of attack. It can be also noticed that the wake region behind each section of the modification is particularly small in comparison with the baseline airfoil at the respective angles of

141

attack and can be considered as implying no considerable effect on the aerodynamic performance of the configurations especially at AoA 8°.

(a)   (b)   (c)

AoA = 8°

(a)   (b)   (c)

AoA = 16°

Velocity   [m s^-1]

0.00 0.38 0.76 1.13 1.51 1.89 2.27 2.65 3.02 3.40 3.78
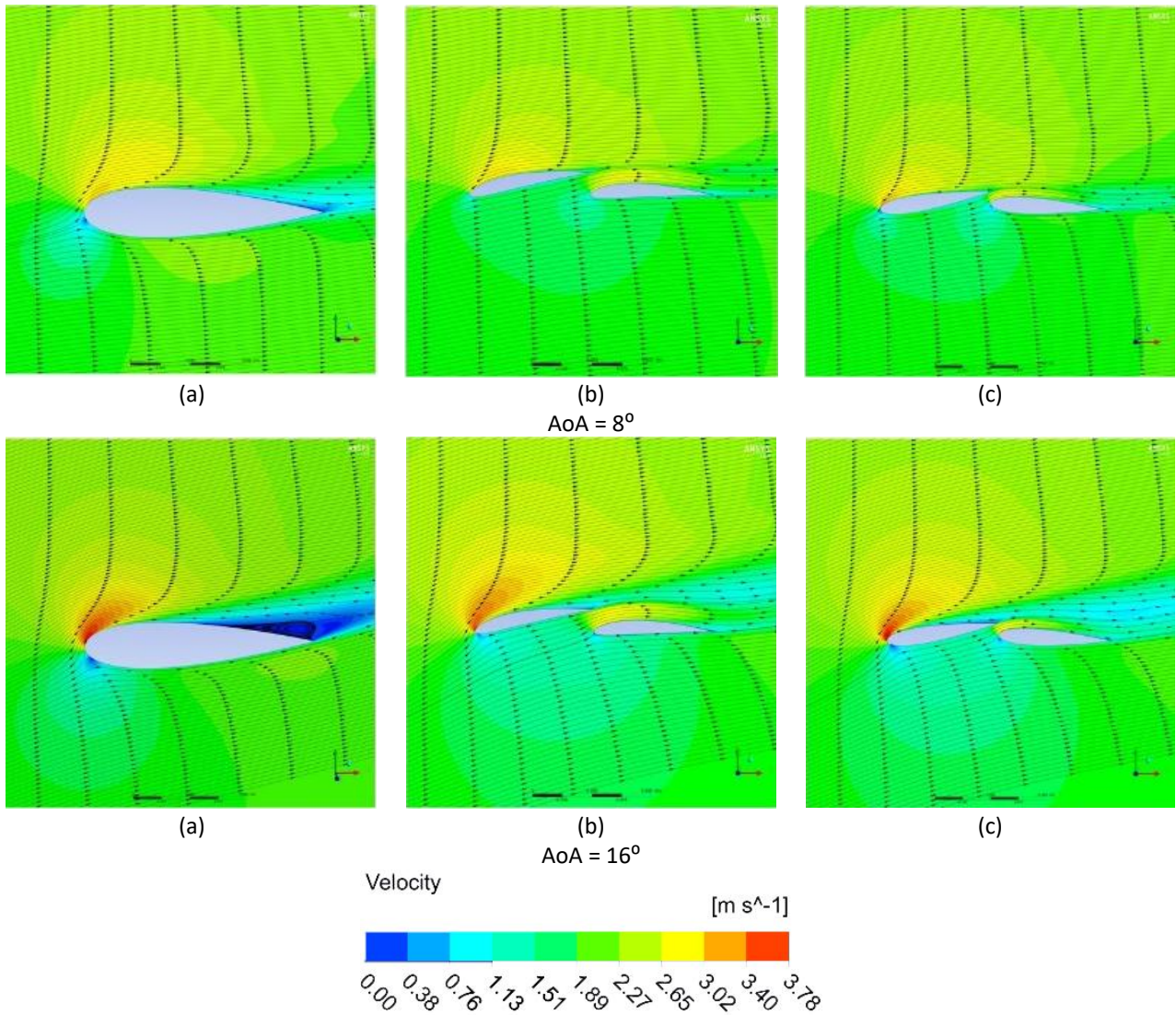
Fig. 22. Velocity Contour and Streamlines for (a) the baseline NACA 0021 airfoil, (b) the cambered configuration and (c) the symmetrical configuration, (d) The velocity range for the contours

Figure 22 shows a significant improvement to the low velocity area at the trailing edge of the baseline airfoil on its upper surface when it comes to the usage of cambered and symmetrical multi element airfoil modification configurations at the relatively low angle of attack of 8° as well as eliminating the wake region that was present after the baseline airfoil at the same angle of attack. There was no separation of flow present on the suction side of the baseline airfoil at AoA 8° as well as the cambered and multi element airfoil modification configurations. On the other hand, at AoA 16, the baseline airfoil experienced a very sharp and early separation loss between the air flow and its suction side as well as a very large low velocity region that expands from the point of separation loss until after the airfoil section. The effect of the implementation of cambered and symmetrical multi element airfoil modification configurations can be shown in Figure 22, and it can be observed that the optimal configurations were able to delay the separation loss phenomena successfully and introduce the entire elimination of it upon three sections of the four sections presented of the modification. At AoA 16, the cambered configuration showed less formation of wake region in

comparison with the symmetrical configuration as well as a smaller low velocity region upon the trailing edge of the first sections while the symmetrical configuration was able to reach higher velocity upon the leading edge of the first sections.

Whenever the velocity is in discussion the coefficient of drag must be considered, and it can be noticed from the graph of coefficient of drag against angles of attack in Figure 18 that the cambered and symmetrical configurations had coefficients of drag that are significantly lower than that of the baseline NACA 0021 airfoil at AoA 8°. This behaviour can be explained to be as a result of dividing the whole baseline airfoil into two smaller sections having lower chord lengths and those sections were also done by the usage of airfoils which had lower maximum thickness in comparison with the baseline NACA 0021 airfoil. The cascade of smaller sections plays a huge role in decreasing the coefficient of drag significantly in two main ways, the first way was built upon the concept of having the two sections separated from each other and this help in allowing the air flow to pass freely in between those two sections permitting for a better aerodynamic shape and performance as shown in Figure 22 and thus, reducing the drag significantly. The second way that help in decreasing the coefficient of drag was built upon the drag formula that states that the drag force is directly proportional to the surface area of the object resisting the air flow and therefore, the optimal configurations were done by using small sections that helped the air flow to pass around smaller two profiles with smaller surface areas in comparison with the huge profile of the baseline NACA 0021 airfoil.

5. Conclusions

In conclusion, this paper provides optimum configurations for using the multi element airfoil modification within the geometrical boundaries of the NACA 0021 using airfoil members of the NACA 4412 cambered airfoil and the NACA 0015 symmetrical airfoil. The numerical simulations were conducted by the usage of CFD Ansys Fluent software at a Reynolds number of 140,000 for a range from 0° to 20° angles of attack and the turbulence model used is the k-ε Standard turbulence model. The optimum configurations of the cambered and symmetrical multi element airfoil modification configurations improved the lift and reduced the drag significantly in comparison with the baseline airfoil. The outcome of this paper can be potentially beneficial for the applications of low wind speeds wind turbines and vertical axis wind turbines. The essential objectives of this paper had been reached and can by summarized in the following statements.

i. The optimal cambered and symmetrical multi element airfoil modification configurations had succeeded in raising the whole glide ratio curves in comparison with the baseline NACA 0021 airfoil.

ii. The optimal cambered and symmetrical multi element airfoil modification configurations had effectively helped in delaying the flow separation phenomena that occur between air flow and the suction side of the baseline airfoil to the extent of nearly eliminating it.

iii. The optimal cambered multi element airfoil modification configurations had achieved a better overall performance when it comes to delaying the separation and raising the whole glide ratio curve in comparison with the symmetrical multi element airfoil modification configurations.

6. Future Work

Finally, it is essential to mention that the authors have further interests in the multi-element airfoil modification in order to deepen the understanding of its effects upon other airfoils, also its application for Darrieus type VAWT.

Acknowledgments

References

[1]   Wirz, Richard, and Perry Johnson. "Aero-structural performance of multiplane wind turbine blades." In *29th AIAA Applied Aerodynamics Conference*, p. 3025. 2011. https://doi.org/10.2514/6.2011-3025

[2]   Roth-Johnson, Perry, Richard E. Wirz, and Edward Lin. "Structural design of spars for 100-m biplane wind turbine blades." *Renewable Energy* 71 (2014): 133-155. https://doi.org/10.1016/j.renene.2014.05.030

[3]   Yavuz, T., E. Koç, B. Kılkış, Ö. Erol, Can Balas, and T. Aydemir. "Performance analysis of the airfoil-slat arrangements for hydro and wind turbine applications." *Renewable Energy* 74 (2015): 414-421. https://doi.org/10.1016/j.renene.2014.08.049

[4]   Ragheb, Adam, and Michael Selig. "Multi-element airfoil configurations for wind turbines." In *29th AIAA Applied Aerodynamics Conference*, p. 3971. 2011. https://doi.org/10.2514/6.2011-3971

[5]   Genç, M. Serdar, Ünver Kaynak, and Gary D. Lock. "Flow over an aerofoil without and with a leading-edge slat at a transitional Reynolds number." *Proceedings of the Institution of Mechanical Engineers, Part G: Journal of Aerospace Engineering* 223, no. 3 (2009): 217-231. https://doi.org/10.1243/09544100JAERO434

[6]   Narsipur, Shreyas, Brent Pomeroy, and Michael Selig. "CFD analysis of multielement airfoils for wind turbines." In *30th AIAA Applied Aerodynamics Conference*, p. 2781. 2012. https://doi.org/10.2514/6.2012-2781

[7]   Timmer, W. A., and R. P. J. O. M. Van Rooij. "Summary of the Delft University wind turbine dedicated airfoils." *Journal of Solar Energy Engineering* 125, no. 4 (2003): 488-496. https://doi.org/10.1115/1.1626129

[8]   Atalay, Kumru Didem, Berna Dengiz, Tahir Yavuz, Emre Koç, and Yusuf Tansel İç. "Airfoil-slat arrangement model design for wind turbines in fuzzy environment." *Neural Computing and Applications* 32, no. 17 (2020): 13931-13939. https://doi.org/10.1007/s00521-020-04796-9

[9]   Zahle, Frederik, Mac Gaunaa, Niels N. Sørensen, and Christian Bak. "Design and wind tunnel testing of a thick, multi-element high-lift airfoil." In *European Wind Energy Conference and Exhibition (EWEA)*, Vienna. 2013.

[10] Eisele, O., and G. Pechlivanoglou. "Single and Multi-element Airfoil Performance Simulation Study and Wind Tunnel Validation." In *Wind Energy-Impact of Turbulence*, pp. 17-22. Springer, Berlin, Heidelberg, 2014. https://doi.org/10.1007/978-3-642-54696-9_3

[11] Chougule, Prasad D., Lasse Rosendahl, and Søren RK Nielsen. "Experimental study of the effect of a slat angle on double-element airfoil and application in vertical axis wind turbine." *Ships and Offshore Structures* 10, no. 2 (2015): 176-182. https://doi.org/10.1080/17445302.2014.918685

[12] Gaunaa, Mac, Frederik Zahle, Niels N. Sørensen, Christian Bak, and Pierre-Elouan Réthoré. "Rotor Performance Enhancement Using Slats on the Inner Part of a 10MW Rotor." In *European Wind Energy Conference and Exhibition (EWEA)*, Vienna, pp. 4-7. 2013.

[13] Jaume, Ana Manso, and Jochen Wild. "Aerodynamic design and optimization of a high-lift device for a wind turbine airfoil." In *New Results in Numerical and Experimental Fluid Mechanics X*, pp. 859-869. Springer, Cham, 2016. https://doi.org/10.1007/978-3-319-27279-5_75

[14] Khan, Sher Afghan, Musavir Bashir, Maughal Ahmed Ali Baig, and Fharukh Ahmed Ghasi Mehaboob Ali. "Comparing the effect of different turbulence models on the CFD predictions of NACA0018 airfoil aerodynamics." *CFD Letters* 12, no. 3 (2020): 1-10. https://doi.org/10.37934/cfdl.12.3.110

[15] Katz, Joseph. *Race Car Aerodynamics: Designing for Speed (Engineering and Performance)*. Bentley Publishers, 1996.

[16] Balduzzi, Francesco, Alessandro Bianchini, Giovanni Ferrara, David Holst, Benjamin Church, Felix Wegner, George Pechlivanoglou, Christian Navid Nayeri, Christian Oliver Paschereit, and Lorenzo Ferrari. "Static and dynamic analysis of a NACA 0021 airfoil section at low Reynolds numbers based on experiments and CFD." In *Turbo Expo: Power for Land, Sea, and Air*, vol. 51180, p. V009T48A004. American Society of Mechanical Engineers, 2018. https://doi.org/10.1115/GT2018-75426

[17] Balduzzi, Francesco, Alessandro Bianchini, Riccardo Maleci, Giovanni Ferrara, and Lorenzo Ferrari. "Critical issues in the CFD simulation of Darrieus wind turbines." *Renewable Energy* 85 (2016): 419-435. https://doi.org/10.1016/j.renene.2015.06.048

[18] Mohamed, Omar S., Ahmed A. Ibrahim, Ahmed K. Etman, Amr A. Abdelfatah, and Ahmed M. R. Elbaz. "Numerical investigation of Darrieus wind turbine with slotted airfoil blades." *Energy Conversion and Management: X* 5 (2020): 100026. https://doi.org/10.1016/j.ecmx.2019.100026